Effect of permeability on the stability conditions of a slope through hydromechanical numerical analyses

Leonardo Ribeiro[1*], Sara Rios[1], António Viana da Fonseca[1], Miguel A. Mánica[2]

[1]*Faculty of Engineering of University of Porto*
Rua Dr. Roberto Frias, 4200-465, Porto, Portugal
*up201800308@up.pt (*corresponding author), srrs@fe.up.pt, viana@fe.up.pt*
[2]*Institute of Engineering, National Autonomous University of Mexico*
Av. Universidad 3004, Copilco Universidad, Coyoacán, 04510 Ciudad de México, CDMX, México
mmanicam@iingen.unam.mx

Abstract. In this work, data from laboratory tests on an iron tailing was used to calibrate the Clay and Sand Model (CASM), a critical state constitutive model able to reproduce the undrained softening behavior that can occur in loose soils. After defining a set of parameters that could reproduce the soil behavior in triaxial compression tests, a simple slope was simulated with the finite element program PLAXIS 2D to evaluate its hydromechanical behavior as a function of the imposed flow conditions. For this purpose, different permeability coefficients were used to evaluate its effect in fully coupled flow deformation analyses. Furthermore, in the case of stratified soil masses, or in the presence of intercalations of materials with different properties, vertical and horizontal permeabilities can vary significantly. Therefore, another objective of the work was to evaluate the effect of the relationship between vertical and horizontal permeabilities on the behavior of the slope, as well as the existence of materials with different permeabilities.

Keywords: slope stability; liquefaction; CASM; permeability ratio; hydromechanical numerical analysis

1 Introduction

Stability analysis of slopes in large landfills (such as earth dams for water storage, road embankments, or structures for deposition of mine tailings), can be conducted by means of hydromechanical stress-strain analyses with the finite element method. If the material is in a loose state and becomes saturated due to heavy precipitation and deficiency in the drainage system, or if it was compacted or deposited with a high water content, it may undergo liquefaction. To evaluate such a condition through numerical analyses it is necessary to use advanced constitutive models capable of simulating the evolution of the material during construction as well as the undrained softening behavior underlying the flow liquefaction phenomenon.

This situation is particularly relevant for mine tailings' piles, where filtered tailings are compacted with higher water contents and lower densities than the standard Proctor optimum. These structures are still associated with large uncertainties, such as their height limits due to very high overburden stresses. The tailings slurry resulting from the mineral extraction is filtered to reduce its water content and transition to a non-segregating state. The material is then compacted in massive embankments. However, it should be noted that the term "dry stack", frequently used for these structures, is a misnomer since the material is not dry. It is in fact in partially saturated conditions, Davies [1], with a degree of saturation of around 70-85% depending on several factors, such as filtration process, type of material, transportation method, and climate conditions, among others.

When the degree of compaction is high (typically above 95% of standard Proctor), filtered tailings show a dilatant response for various confining stresses. However, for lower degrees of compaction, the response becomes contractive, particularly at medium to high confining pressures. Additionally, when the material is less compacted and/or on the wet side of the compaction curve, it may become saturated when subjected to high effective stresses due to the rise of the embankment. Depending on the permeability and mineralogy of the material, and on the loading rate related to subsequent rises, excess pore pressures can be generated in the embankment, mobilizing low undrained strength ratios, far from critical state conditions, eventually dropping to post-peak residual values in a non-Newtonian behavior, Gens [2]. Additionally, the water table rise due to heavy rain or inefficient drainage creates a flow of water along the slope that can trigger an unstable condition depending on soil permeability and percolation time.

Within this context, the present work aims to evaluate the effect of permeability on the stability conditions

of a slope by means of fully coupled hydromechanical finite element analyses. Particularly, simulations are intended to reproduce a physical model, that is scheduled to be tested in a geotechnical centrifuge, representing a 31 m high slope of a dry stack tailings facility. Therefore, in this case, the study is not focused on the evaluation of stability during embankment construction but on the slope stability during water flow. The constitutive model adopted, briefly described below, can successfully characterize the behavior of the loose iron tailings considered in this research, including the undrained softening behavior associated with flow liquefaction. Analyses were also performed to evaluate the effect of permeability anisotropy, which might occur because of the compaction procedure. Obtained results provide relevant insights into the importance of permeability in the evaluation of stability conditions in tailing storage facilities or similar structures.

2 Clay and Sand Model (CASM)

2.1 Formulation

CASM is a constitutive model developed by Yu [3], formulated within the framework of the critical state theory. It is based on the concept of the state parameter ψ, defined as the difference between the initial void ratio and the void ratio on the critical state line (CSL) for the same mean effective stress p'. CASM is an elastoplastic strain hardening model, with the same hardening rule as the modified Cam Clay, defined in terms of the volumetric plastic strain ε_v^p:

$$\frac{dp_0'}{p_0'} = \frac{1+e}{\lambda-\kappa} d\varepsilon_v^p \,, \tag{1}$$

where p_0' is the initial effective consolidation pressure, e is the initial void ratio, and λ and κ are the slopes of the CSL and the unloading/reloading line, respectively.

CASM was originally formulated as an extension of the Cam-Clay model, Roscoe et al. [4], with a yield function defined by the following expression:

$$f = \left(\frac{q}{p' M_\theta}\right)^n + \frac{1}{\ln r} \ln\left(\frac{p'}{p_0'}\right), \tag{2}$$

where q is the deviatoric stress, M_θ is the slope of the CSL in the $q - p'$ space, which depends on the Lode angle θ, and n and r are material parameters controlling the shape of the yield function.

For the plastic potential function, the following expression was adopted, according to Mánica et al. [5]:

$$g = \left(\frac{q}{p' M_\theta}\right)^m + m - \frac{p_c'(m-1)}{p'} - 1 \tag{3}$$

where p_c' must be solved for the current stress state and m controls the shape of the function, and can be determined with eq. (4) in terms of the coefficient of earth pressure at rest K_0:

$$\frac{9(\lambda-\kappa)(2\nu-1)}{2\kappa\eta_{K_0}(\nu+1) + 6\lambda(2\nu-1)} = \left(\frac{M}{m} - M\right)\frac{\eta_{K_0}}{M} + \left(M - \frac{M}{m}\right)\left(\frac{\eta_{K_0}}{M}\right)^{1-m} \tag{4}$$

where η_{K_0} is the stress obliquity ratio for K_0 conditions and M is the slope of the critical state line for triaxial compression, which can be related to the critical state friction angle as $\sin\phi_{cs} = 3M/(6+M)$.

The elastic behavior of the model follows the same nonlinear elasticity as the modified Cam Clay, where the bulk modulus K depends on the mean effective stress and it is defined in terms of κ.

2.2 Calibration procedure

CASM requires nine input parameters, indicated in Tab. 1, from which λ, Γ, and ϕ_{cs} are well-known from critical state soil mechanics; they were obtained from conventional triaxial tests performed on an iron tailing material. Parameters r and n were determined following the procedure proposed by Mánica et al. [5], in terms of the undrained peak strength ratio $S_p = s_u/p'$. Furthermore, since a loose state of the material is being considered, normally consolidated conditions were adopted, i.e., R = 1. Finally, to characterize the elastic behavior, values of 0.3 and 0.005 were assumed for ν and κ, respectively.

Table 1. Summary of parameters adopted for CASM

Symbol	Description	Value	Unit
λ	CSL slope in the compression plane	0.039	-
κ	Unloading/reloading slope in the compression plane	0.005	-
ν	Poisson ratio	0.300	-
ϕ_{cs}	Internal friction angle on Critical State	33.32	°
n	Yield function shape parameter	1.262	-
r	Yield function shape parameter	4.742	-
m	Plastic potential function parameter	2.920	-
Γ	CSL position in the compression plane	2.009	-
R	Overconsolidation ratio	1.000	-

3 Numerical model

Numerical analyses were intended to simulate a slope similar to the one that will be assessed through physical modelling in a geotechnical centrifuge at Deltares, Netherlands, within the context of the SAFETY Project, conducted with European funds through H2020 GEOLAB consortium (https://project-geolab.eu/). The objective of this project is to analyze the stability of tailings piles containing loose soils, subjected to seepage flow which can trigger an undrained failure.

The considered geometry corresponds to a slope of a dry stack, with an inclination of approximately 30º, and with the dimensions shown in Fig. 1. The upstream and downstream berms extend horizontally 20 and 13.5 m, respectively. There is also a blanket drain at the bottom right corner, 17.2 m in length. These dimensions are approximately those that the physical model aims to represent at a scale of 1:100.

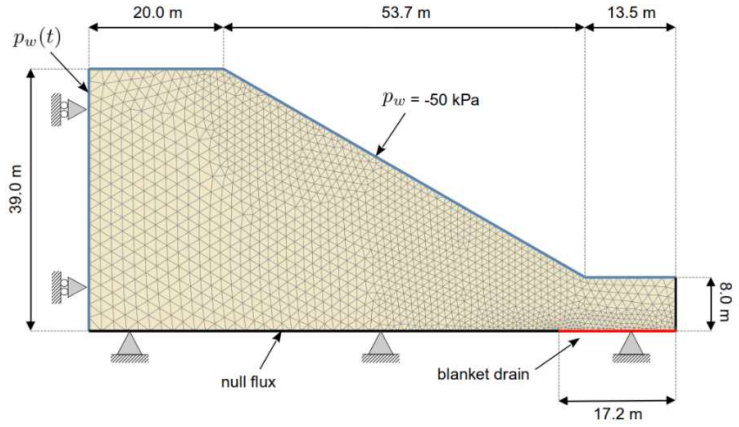

Figure 1. Geometry, mesh, and boundary conditions adopted.

3.1 Phases of calculation

A fully coupled hydromechanical analysis, using the CASM constitutive model, was performed to simulate the behavior of the embankment. The analysis comprises three calculation phases: (1) a simple equilibrium calculation with the Mohr-Coulomb constitutive model, where body forces are activated to generate the initial stress state; (2) a phase to change the material to CASM and verify equilibrium; and (3) and a hydromechanical computation where the phreatic level is gradually raised from 0 to 30 meters during a time interval of 30 minutes.

3.2 Mechanical and hydraulic boundary conditions

Figure 1 also shows the main mechanic and hydraulic boundary conditions adopted. At the left and right boundaries, displacements were restrained only in the horizontal direction, while at the bottom boundary, both vertical and horizontal displacement components were constrained. As for hydraulic conditions, a suction value of

50 kPa, based on the retention curve of the soil adopted, was applied at the free surface of the model to account for the partially saturated conditions at the beginning of the test. At the left boundary, a liquid pressure varying linearly with depth was prescribed to define initial conditions, from a suction of 50 kPa at the crest of the slope to a zero liquid pressure at the bottom of the model. This boundary was then modified in the last phase to account for the gradual rise of the water table, up to 30 m in 30 minutes. The latter was achieved by increasing the liquid pressure with time to obtain a zero liquid pressure at a height of 30 m and a positive pressure of 300 kPa at the base of the model at this boundary. Finally, the blanket drain was simulated by imposing a zero liquid pressure on the red line indicated in Fig. 1.

4 Results

4.1 Variation of permeability

An initial set of analyses was performed assuming an isotropic permeability, i.e., $k_x = k_y$. Six different values of permeabilities (from $5x10^{-4}$ to $1x10^{-6}$ m/s) were used to evaluate the effect of this parameter on the results. Table 2 summarizes the obtained maximum displacements (norm) and deviatoric strains for the different permeability values considered. The results show an increase in both displacements and deviatoric strains as the permeability was increased from $1x10^{-6}$ to $5x10^{-5}$ m/s. Although in all cases the calculation phase was completed, for permeability values above $5x10^{-5}$ m/s quite high displacements and strains were obtained suggesting that the slope is approaching an unstable condition. There is a small decrease in displacements and strains for the two largest permeabilities, although values are still significantly larger compared to the analyses with smaller permeabilities.

Table 2. Summary of results for the variation of permeability

Permeability [m/s]	Max. displacements [cm]	Total deviatoric strain [%]
$5x10^{-4}$	41.55	2.61
$1x10^{-4}$	61.39	3.98
$5x10^{-5}$	65.04	4.26
$1x10^{-5}$	9.87	0.98
$5x10^{-6}$	0.86	0.27
$1x10^{-6}$	0.13	0.10

Figures 2 and 3 show the contours of total displacements and deviatoric strains, respectively, for the different permeabilities at the end of the simulation. The phreatic surface is also depicted in the figures. As already suggested, the onset of a failure mechanism can be identified in the analyses with permeabilities equal to or larger than $1x10^{-5}$ m/s. The latter can be explained in terms of the propagation of the phreatic surface, which reduces effective stress and, therefore, reduces the strength of the soil. While for high permeability values the phreatic surface ends up close to the steady-state condition, in the analyses with small permeability values the phreatic surface does not propagate much and, therefore, a higher strength operates in a larger portion of the domain resulting in smaller displacements and strains. However, it is important to notice that the latter more stable condition is transitory and, eventually, the phreatic surface will achieve steady-state conditions if the analysis is run for a sufficient time, leading to higher displacements and strains.

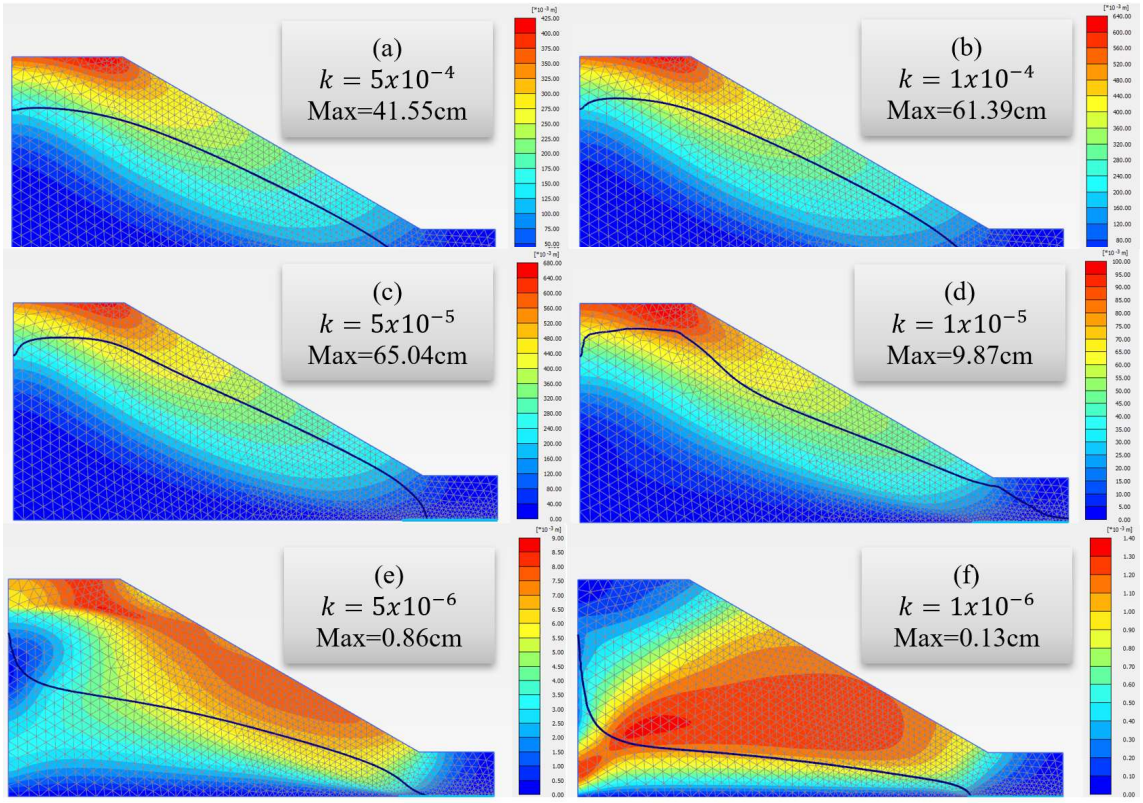

Figure 2. Total displacements for the analyses with permeability values k of (a) $5x10^{-4}$, (b) $1x10^{-4}$, (c) $5x10^{-5}$, (d) $1x10^{-5}$, (e) $5x10^{-6}$, and (f) $1x10^{-6}$ m/s.

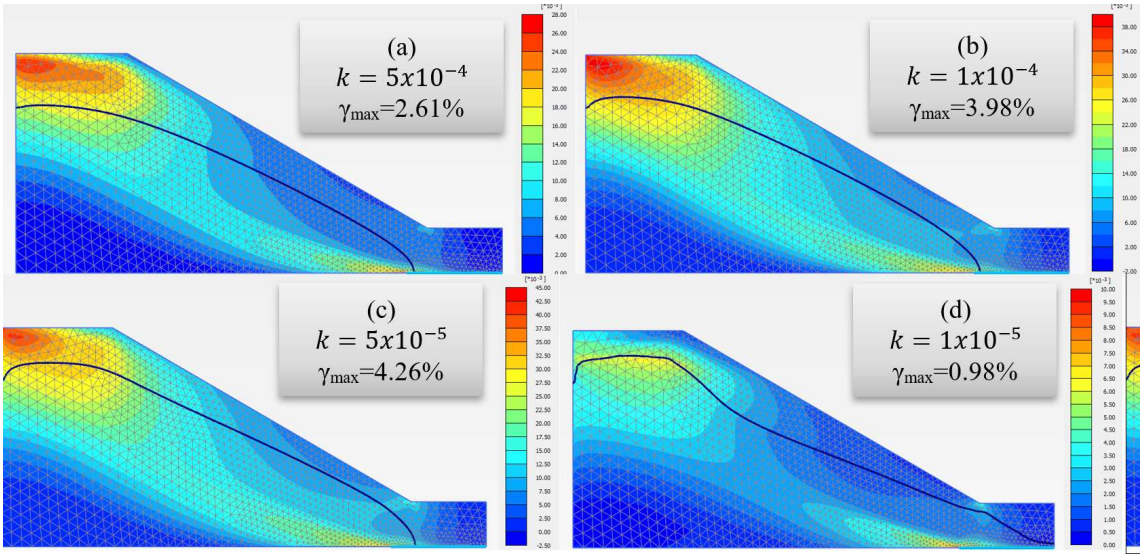

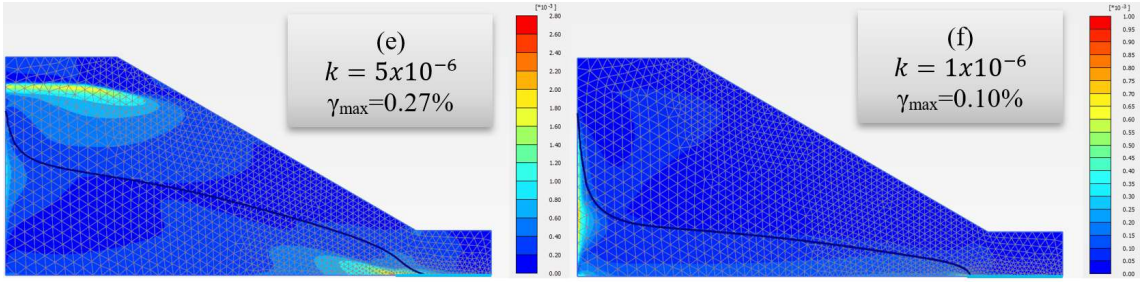

Figure 3. Total deviatoric strains for the analyses with permeability values k of (a) $5x10^{-4}$, (b) $1x10^{-4}$, (c) $5x10^{-5}$, (d) $1x10^{-5}$, (e) $5x10^{-6}$, and (f) $1x10^{-6}$ m/s.

The stress path followed at different locations during water percolation was also analyzed for the different permeability values. Figure 4a indicates the location of the considered integration points, while Fig. 4b, 4c, and 4d compare the resulting stress paths with respect to the CSL; the influence of permeability is evident. In point 4139 (Fig. 4b), the increase in water pressure causes the stress paths to move to the left towards the CSL. For lower permeabilities, there is some decrease of the deviatoric stress, although the stress path barely reaches the CSL. For higher permeabilities, the stress paths reach the CSL, and, because of the higher dissipation rates, strength can increase somewhat along the CSL. However, the latter results in the accumulation of plastic deformations. On the other hand, in point 12688 (Fig. 4c), there is a significant decrease of the deviatoric stress driven by the increase of water pressures, the latter being more pronounced as the permeability increases due to higher dissipation. Finally, in point 29997 (Fig, 4d), there is an increase in the mean and the deviatoric stresses for all cases. However, since this point is adjacent to the drain, water pressure barely changes at this location and, therefore, the increase of the mean stress occurs also in terms of total stresses, caused by stress redistributions generated during water percolation and the propagation of the phreatic surface.

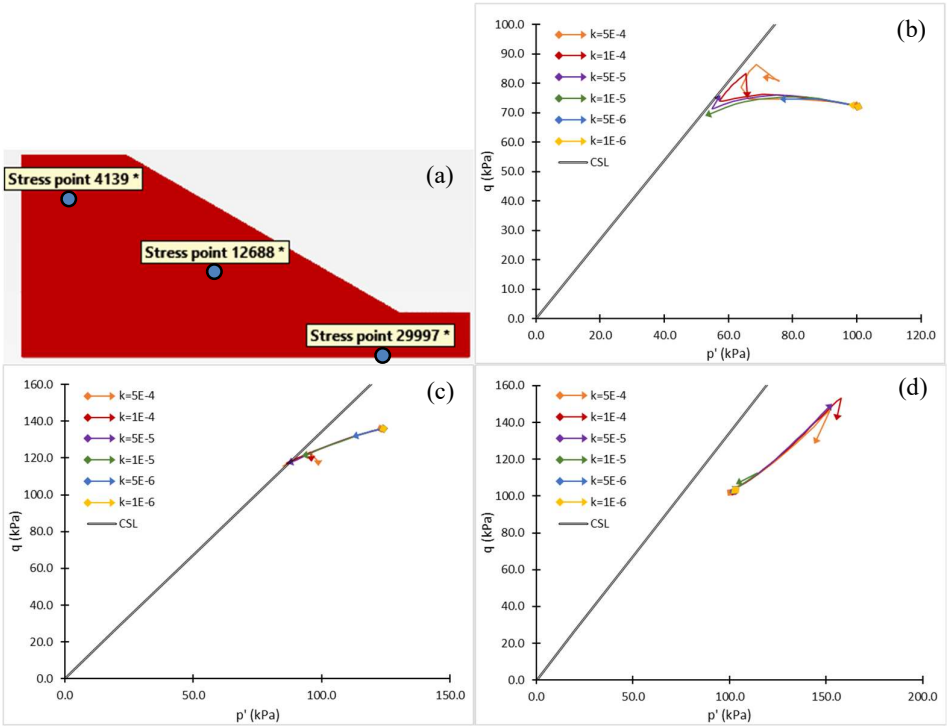

Figure 4. (a) Position and stress paths for the integration points (b) 4139, (c) 12688, and (d) 29997.

4.2 Effect of permeability anisotropy

An additional analysis was also performed with the same conditions (parameters, phases, and boundary

conditions) but assuming a horizontal permeability equal to twice the value of the vertical permeability, using values of $2x10^{-5}$ and $1x10^{-5}$ m/s for the horizontal and vertical directions, respectively. Figure 5 shows the resulting contours of (a) total displacements and (b) deviatoric strains; the phreatic surface is also depicted in the figure. It is evident that dissipation is enhanced compared to the analysis with an isotropic permeability of $1x10^{-5}$ m/s, resulting in a phreatic surface closer to steady-state conditions. However, even though the average permeability is larger than the mentioned analysis, displacement and strains are smaller, suggesting that permeability anisotropy plays a significant role in the hydromechanical behaviour of the slope.

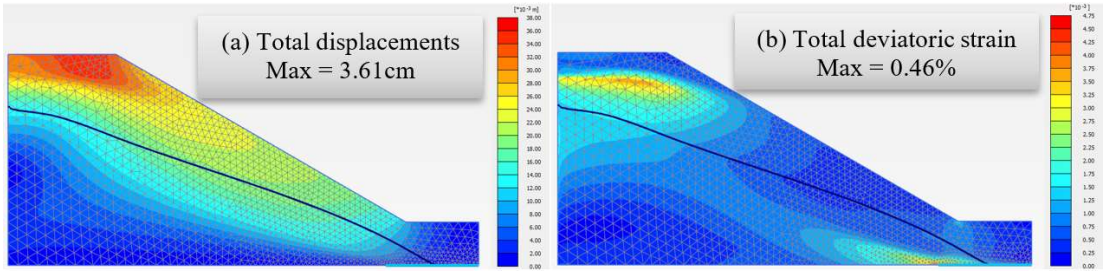

Figure 5. (a) Total displacements, (b) total deviatoric strains for $k_x = 2x10^{-5}$ and $k_y = 1x10^{-5}$ m/s.

5 Conclusions

This numerical work aimed at demonstrating the influence of permeability on the stability conditions of a slope embankment using CASM constitutive model and fully coupled hydromechanical analysis in PLAXIS. Since the percolation time was fixed at 30 min., an increase in the soil permeability led to higher displacements and shear strains as the phreatic surface could reach a larger domain of soil in the slope. For higher permeability values, the slope approached an unstable condition where the onset of a slip surface was identified, together with large displacements. Similar results could have been obtained with higher percolation time and lower permeability, as these variables are related. The results highlight that seepage flow through a slope can induce failure depending on the soil permeability, including its anisotropic characteristics, and percolation time. Since *in situ* permeability is often difficult to estimate, especially horizontal permeability, conservative design must be adopted, including parametric analyses based on reliable laboratory data to calibrate advanced constitutive parameters.

Acknowledgments: This work was financially supported by: Base Funding - UIDB/04708/2020 of the CONSTRUCT - Instituto de I&D em Estruturas e Construções, by the project INPROVE-2022.02638.PTDC, and by CEECIND/04583/2017 grant to the 2nd author, from national funds through the FCT/MCTES (PIDDAC).

Authorship statement. The authors hereby confirm that they are the sole liable persons responsible for the authorship of this work, and that all material that has been herein included as part of the present paper is either the property (and authorship) of the authors or has the permission of the owners to be included here.

References

[1] M. Davies, "Filtered Dry Stacked Tailings – The Fundamentals". *Proc. Tailings and Mine Waste, Vancouver*, 2011.
[2] A. Gens. "Hydraulic fills with special focus on liquefaction*". XVII ECSMGE-2019: Geotechnical Engineering foundation of the future*, pp. 1-31. https://doi.org/10.32075/17ECSMGE-2019-1108, 2019
[3] H. S. Yu, CASM: "A unified state parameter model for clay and sand". *International Journal of Numerical* and Analytical Methods in Geomechanics, No. 22, 621-653, 1998.
[4] K. H. Roscoe, A. N. Schofield, and A. Thurairajah, "Yielding of Clays in States Wetter than Critical" *Géotechnique,* 13(3), pp. 211-240, 1963.
[5] M. A. Mánica, M. Arroyo, A. Gens, and L. Monforte, "Application of a critical state model to the Merriespruit tailings dam failure". Proceedings of the Institution of Civil Engineers - Geotechnical Engineering, 175(2), pp. 151-165